Manoj KUMAR, PhD (corresponding author)
manoj1985.111@gmail.com
Jaypee University of Engineering and Technology, India

Manish KUMAR PATIDAR, PhD
manish.patidar@juet.ac.in
Jaypee University of Engineering and Technology, India

Narendra SINGH, PhD
narendra.singh@juet.ac.in
Jaypee University of Engineering and Technology, India

Channel Capacity Enhancement with Nonlinear Distorted Signal Detection Using OFDM-NOMA Systems with Optimization System

Abstract. *The integration of Non-Orthogonal Multiple Access (NOMA) techniques with Orthogonal Frequency Division Multiplexing (OFDM) in 6G networks, aiming to reduce frequency selectivity in multipath channels. It highlights the challenges faced by OFDM signals in nonlinear High-Power Amplifiers (HPA) due to their high Peak-to-Average Power Ratio (PAPR). The study explores the potential of Massive Multiple-Input Multiple-Output (MIMO) technology, particularly in millimeter-wave (mmWave), to enhance energy and spectrum efficiency, productivity, and capacity in communication systems. The research proposes a Fuzzy Firefly Algorithm (FFA) trained with Radial Basis Function Neural Networks (RBFNN) for non-linear channel equalisation, and a Particle Filter (PF) based iterative approach for distortion compensation and interference cancellation in nonlinear data detection.*

Keywords: *Non-Orthogonal Multiple Access, nonlinear distorted signal, Peak Signal-to-Noise Ratio, BER, Radial Basis Function, SWIPT.*

JEL Classification: O3, R4, Y1.

1. Introduction

The Fifth Generation (5G) technology was formed to satisfy the stringent device and service requirements of both new and established networks. Future connected enterprises will exhibit a considerable increase in bandwidth and network densification, traffic density, and an extensive variety of novel technologies and applications (Zhang et al., 2021). To meet the requirements for higher network capacity, more effective custom of spectrum, higher user data rates, more reliability, lower latency and power consumption, and higher link capacity, the efficiency envelope of wireless networks needs to be pushed to new limits through the software-defined network (SDN) and network function virtualisation (NFV) (Ali and Yahya, 2022). Nevertheless, the usage of MIMO in 5G wireless technology will lead to

DOI: 10.24818/18423264/58.2.24.06

lower energy efficiency (EE) and increased circuit power consumption (Qamar et al., 2022). Using OFDM, the network's data transmission has been conducted. In MMU-MIMO, the base station effectively provides service to multiple customers concurrently using the same frequency (Wu et al., 2022).

The FSI-OFDM method offers the ability to adaptively allocate sensing resources, providing a solution for the mentioned challenges. FSI-OFDM improves both simple self-interference (SI) cancellation and superseding range (SSR) (Mal et al., 2021). In (Vaigandla and Benita, 2022), OFDM and Filter Bank Multi-Carrier (FBMC) transmission approaches are compared. The Spectral Density, SE, PAPR, as well as Bit Error Rate (BER), are used to compare the benefits of OFDM and FBMC inflexion schemes. Some OFDM flaws are addressed by FBMC (Ding et al., 2021). The ability to handle channel symbols of the 5G standard utilising FBMC signals in combination with already existing code sequences and algorithms, allows for an increase in the SE of the baseband signal and an increase in transmission rate by eliminating of the cyclic prefix (Butenko et al., 2021).

A cutting-edge quasi-space-time block codes (STBC) encoder for OFDM systems has been developed, ensuring optimal data transfer rates in MIMO communication (Zheng et al., 2021). The potential benefit of complementary the trade-off surrounded by EE and SE has recently drawn more attention to MIMO-OFDM with index modulation. Singh and Kumar (Singh and Kumar, 2022) suggested a workable approach to roughly attain an internationally Pareto-optimal trade-off among SE and EE, enduring usage of the Pareto-optimal beam strategy, and demonstrated that the collision limitations of the multi-objective optimisation problem (MOP) also addressed rapidly.

The work's discontinuity is structured in the following manner: Section 2 presents the literature review, Section 3 delves into the problem definition and research motivation, and Section 4 outlines the proposed research methods. Section 5 exhibits the experimentation and result discussion, and Section 6 accomplishes the study.

2. Literature Survey

The primary design aim in cellular and wireless communication engineering is to build a wireless CS that uses little spectrum and little power. To address next-generation cellular CSs beyond 5G and 6G, Hossain (Hossain et al., 2022) proposed a high-throughput cellular CSs named restructuring with discrete Fourier transform-spread Restructuring and Windowing OFDM, which has exceptionally low PAPR and low OOB power emission.

Zhang et al (2022) offer a compressive OFDM system, concentrating on the advanced SE need. To produce the compressive OFDM signal, the proposed system applies a truncation filter to the OFDM signal with a purposefully chosen compression ratio and truncation mode. To recharge from the faulty signal reception, up-sampling and recurring predictions are utilised. Furthermore, the suggested compressive OFDM system has an advantage over SEFDM in terms of spectrum

efficiency. To examine the nonlinear impact of LED on the trade-off concerning EE and SE, the direct current biased optical (DCO-OFDM) was used (Hei et al., 2022). Predistortion compensation techniques were formed to analyse the BER influenced by LED parameter changes, and the Rapps model was utilised to represent the nonlinear feature of commercial LED. This acted as avaluable guide to select the most effective system settings for the nonlinear DCO-OFDM VLC method.

The crucial step in reducing the cost and complexity of multi-user mmWave MIMO-OFDM systems is the blended precoding reaching a satisfactory sum rate. These methods either perform less than optimally or suffer from higher complexity. Unnisa and Tatineni (2022) suggested the adaptive DL approach for mm-wave M-MIMO-OFDM CS sparse channel estimation (SCE) and the precoding hybrid. The findings show that twisted SCE and mixture pre-coding in mmWave massive MIMO-OFDM CS outperformed existing methods, resulting in superior error rates and increased spectral efficiency. Kumar and Rao (2022) proposed the MIMO-OFDM technique for moveable hypermedia CSs. In the MIMO-OFDM portable combination CS, EE was improved using a hybridised optimisation approach known as Hybrid Fruit Fly-based Swarm Optimisation.

The main difficulties, especially given the rise in user numbers, include spectrum scarcity and high data rates. Sidiq et al (2022) introduced a ground-breaking signal processing approach inspired by nature, which combines the intelligence of UFMC with the innovative GFDM technique to overcome challenges in communication systems. Ali and Yahya (2022) innovatively created a cutting-edge enterprise waveform called F-OFDM, incorporating four sub-bands of different sizes, seven unique window sync screens, and a variety of numerology designs to enhance spectral efficiency.

Singh and Kumar (Singh and Kumar, 2022) generated a new quasi-STBC encoder for OFDM systems while maintaining a full rate in MIMO communication. This proves that one can achieve a high level of flexibility with full disclosure by employing four transmit antennas on the top using the Alamouti scheme, which was previously limited to binary communication antennas for STBC.

3. Research Problem Definition and Motivation

OFDM-based systems are intriguing due to their enhanced ability to combat multipath interference in wireless networks through the use of Fast Fourier Transform techniques. With WLAN (Wireless Local Area Networks) values, WiMax (Worldwide Interoperability for Microwave Access), DAB (Digital Audio Broadcasting), and DVB (Digital Video Broadcasting), OFDM consumes remained selected for Long Term Development networks. Owing to its multipath disappearing resistance and great bandwidth efficiency, the OFDM modulation technique has been adopted for high-speed wireless communications. In OFDM, inward high-speed signals are successively to parallelly translate into N low-haste data streams, resulting in a flat fading for each of the symbol streams.

4. Proposed Research Methodology

OFDM, a dominant 5G wireless technology, offers high data rates and spectrum efficiency. However, it faces issues such as channel misrepresentation, CFO, SFO, and fading. NOMA-based OFDM schemes are attractive for future wireless communication, including 5G, due to massive connectivity, high spectral efficiency, and resistance to frequency selectivity. The planned work's flow diagram is shown in Figure 1.

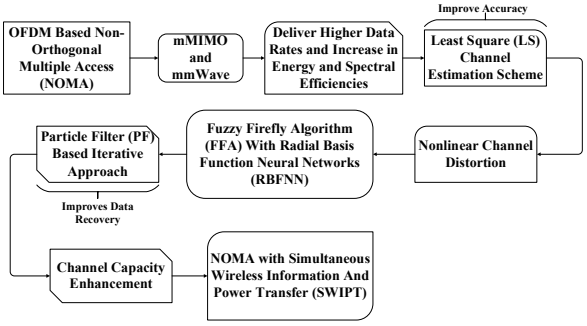

Figure 1. Block Diagram of the Proposed Work

Source: Data collected through the integration of NOMA-OFDM in 6G networks, addressing challenges posed by nonlinear High-Power Amplifiers (HPA) and frequency selectivity in multipath channels is adopted from (Rahman et al., 2023).

This study analyses DL-NOMA-OFDM, focusing on nonlinear properties caused by a polynomial HPA without memory. It highlights the benefits of mmWave systems using MIMO OFDM for spectral efficiency and robustness. Combining mMIMO and mmWave technologies can improve speed, capacity, energy, and spectral efficiency. The Symbol Error Rate (SER) and Least Square (LS) estimation scheme improve wireless communication performance.

4.1 OFDM-Non Orthogonal Multiple Access (NOMA) System

Consider a DL-OFDM-NOMA scheme in which the spreader at the BS covers data from M operators on a similar subcarrier, as different to an OFDM-OMA organisation in which data after a single user is conveyed on an individual subcarrier. The multifaceted baseband depiction of the BS's communicated OFDM-NOMA indication is given by

$$x_n = \frac{1}{\sqrt{N}} \sum_{k=1}^{K} \left(\sum_{m=1}^{M} \sqrt{\alpha_{k,m} P_k A_{k,m}} \right) e^{-j\frac{2\pi nk}{N}} 0 \leq \mathrm{n} \leq \mathrm{N} - 1 \quad (1)$$

In OFDM-NOMA, K represents the SC in a symbol, M is the number of superposed users per subcarrier, and N denotes period sphere models. A block diagram represents the DL OFDM-NOMA system. A block diagram representation of the DL OFDM-NOMA system. At the m^th user's terminal, the received indication on the kth subcarrier is given by:

$$Y_{k,m} = H_{k,m} \left(\sum_{m=1}^{M} \sqrt{\alpha_{k,m} P_k A_{k,m}} \right) + N_{k,m} 1 \leq \mathrm{k} \leq \mathrm{K}, 1 \leq \mathrm{m} \leq \mathrm{M} \quad (2)$$

N_(k,m) represents AWGN for m^th user on subcarrier k, with zero mean and variance σ^2_(k,m). Channel frequency response H_(k,m) is given by g_(k,m)/√(1+d_m^∝). The normalised achievable data rate for the m^th user is calculated.

$$R_m = \sum_{k=1}^{K} log_2(1 + \gamma_{k,m}) \quad (3)$$

where,

$$\gamma_{k,m} = \frac{P_k|H_{k,m}|^2\alpha_{k,m}}{(P_k|H_{k,m}|^2\sum_{i=1}^{m-1}\alpha_{k,m}+\sigma^2{}_{k,m}} = \frac{P_k|H_{k,m}|^2\alpha_{k,m}}{(P_k|H_{k,m}|^2\sum_{i=1}^{m-1}\alpha_{k,m})+1}, \quad (4)$$

Where, $\gamma_{k,m}$ and $p_{k,m} \triangleq P_k/$are the signal-to-interference-plus-noise ratio (SINR) and the SNR of the m^{th}user over the k^{th}subcarrier, respectively. The first time in the denominator of (3) becomes 0 in$\gamma_{k,1}$, i.e., at NU. Finally, the total sum-rate capacity is computed as shown below.

$$R_{Total} = \sum_{m=1}^{M} R_m = \sum_{m=1}^{M} log_2 \prod_{k=1}^{k}\left(1 + \frac{P_{k,m}|H_{k,m}|^2\alpha_{k,m}}{(P_{k,m}|H_{k,m}|^2\sum_{i=1}^{m-1}\alpha_{k,i})+1}\right), \quad (5)$$

MmWave M-MIMO combines mmWave spectrum utilisation and MIMO-OFDM systems to enhance spectral efficiency and channel robustness. By integrating mMIMO and mmWave, it offers increased throughput, capacity, energy, and spectrum efficiency.

4.2 Nonlinear Channel Distortion in OFDM

Non-linear falsifications due to HPA at transmitters of the MIMO CS are single of the foremost sources of Low SNR (Signal Noise Ratio). Accordingly, the research proposed an FFA trained with RBFNN applied for non-linear channel equalisation.

4.2.1 Fuzzy Firefly Optimisation Algorithm (FFA)

M-MIMO mmWave networks exhibit distinct propagation characteristics compared to legacy cellular systems. At mmWave frequencies, channels can become deterministic as the number of base station antennas increases, leading to asymptotic orthogonality for different users.

$$\psi(s) = \frac{1}{\left(\frac{f(g_s)-f(g_h)}{\beta}\right)} \quad (6)$$

Here, the fitness function is $f(g_s)$ for n−brighter fireflies. To eliminate reliance on the fitness function's scale, consider β is represented as follows.

$$\beta = \frac{f(g_h)}{m} \quad (7)$$

To calculate the distance of fireflies' expenditure Cartesian distance which same as FFA. As far as movement is concerned, consider equation (8) in place of (6).

$$x_i = a_i + \beta_{0e}{}^{-\gamma d^2{}_{ij}}\left(a_j - a_i\right) + \alpha\left(rand - \frac{1}{2}\right) + \sum_{s=1}^{n}\psi(s)\beta_{0e}{}^{-\gamma d^2{}_{ij}}(a_s - a_i)\,\alpha\left(rand - \frac{1}{2}\right) \quad (8)$$

In the above expression a_i represents the spatial location of the fewer cheerful firefly, the second component is attributable to the magnetism of the optimistic firefly, and the third period is a fuzzy adjustable representative of the quantity of appeal of n-brighter fireflies in the progression of the fireflies.

FireFly Algorithm Construction and ANN Training

This research trains ANN with FFA to create a population-based network for channel state estimation. It uses training data with ±1 values and calculates fitness via MSE in Equation (9). The 30-network population performs well in equalising challenging control factors.

$$Value\ of\ Fitness = \sum Recorded\ Value - Predicted\ value\ of\ Network \quad (9)$$

When a network has met any minimal execution requirements, it is regarded to be available. The condition was the quantifiable calculation known as the correlation coefficients, which are shown in equation (10).

$$\mu^2 = 1 - \frac{Value\ of\ Fitness}{\sum Recorded\ Value - Mean\ Recorded\ Value} \quad (10)$$

The complexity of the firefly algorithm, in this case, will be$O(n\ t\ log(n))$, where uniform distribution at time t.

4.2.2 Radial Basis Function Neural Network (RBF-NN) Based Equaliser

Unlike F-NN whose hidden neurons (HN) calculate the weighted sum of the input vectors, RBF-HNs calculate the Euclidean detachment among the weight vectors and the input vector. To be more specific, the production of the HNs. $H^{[1]} = [H_1^{[1]}, H_2^{[1]}, \ldots\ldots, H_{n^{[1]}}^{[1]}]^T$maybe intended as

$$H_i^{[1]} = f^{[1]}\left(b_i{}^{[1]}\left|\left|\left(w_i^{[1]}\right)^T - X\right|\right|\right), i = 1,2, \ldots.n^{[1]}, \quad (11)$$

Where, $w_i^{[1]}$is the i-th row vector of the weight matrix $w^{[1]}$ following the notation used for F-NN, and the commonly-used activation function for radial basis HNs is $f^{[1]}(x) = e^{-x2}$.

$$y = f^{[2]}(w^{[2]}H^{[1]} + b^{[2]}) \quad (12)$$

RBF-NN consists of only 2 layers, but F-NN can contain many hidden layers (deep NN). Same as F-NN, when RBF-NN has only a single neuron in the output layer, the number of multiplications needed to recuperate one symbol $N_{mul_{RBF-NN}}$ is given in equation (13).

$$N_{mul_{RBF-NN}} = (n^{[0]} + 2)n^{[1]} \quad (13)$$

As shown in equation (13), the FP step for RBF-NN involves more computational complexity (CC) related to F-NN when a similar quantity of input and HNs are used. The complexity difference is also very small as reduces the quantity of concealed neurons.

4.3 Particle Filter (PF) Based Iterative Approach

At the transmitter, a binary encoder (ENC) is first encoded by information bits and then randomly interleaved. Coded minutes are mapped to a sequence of N modulated symbols $X = [X_1, X_2, \ldots., X_N]^T$using a constellation $S \equiv \{s_j, j = 1,2, \ldots., 2^B\}$ with average power normalised to one. An Inverse Discrete Fourier Transform (IDFT) is then applied, which is expressed as equation (14).

$$x = F^{\dagger}X \qquad (14)$$

Where F is the $N \times N$ unitary discrete Fourier transform (DFT) matrix and $(.)^{\dagger}$ denotes conjugate transpose. A clipping function is defined by the following equation (15).

$$f(x_i) = \begin{cases} Ax_{i/}|x_i|, & |x_i| > A \\ x_i, & |x_i| \le A \end{cases}, (15)$$

The clipping threshold is A > 0, where it is. To keep things simple, we will not perform the typical OFDM procedures of adding and removing cyclic prefixes. The time-domain received signal r is given in equation (16).

$$r = F^{\dagger} \wedge F.f(x) + w, \quad (16)$$

Where, $w \sim CN(0, \sigma^2 I)$a sequence of independent is identically distributed (IID) Gaussian noise and $\wedge = diag\{H_1, H_2, \ldots., H_N\}$is a slanting matrix with $H_i$being the channel coefficient on the $i - th$ subcarrier. Applying DFT to r, obtain a frequency-domain signal vector R in equation (17).

$$R = \wedge F.f\left(F^{\dagger}x\right) + w \qquad (17)$$

Where $W = Fw$ contains Gaussian noise samples. The clipping function $f(\cdot)$ is nonlinear, which makes character discovery challenging. To circumvent this difficulty, linearise $f(x)$ is given in the following equation.

$$f(x) = \alpha x + d) \ (18)$$

Where α is a constant scalar and $d = f(x) - \alpha x$ is the clipping distortion. Substituting (18) to (17) in the following equation.

$$R = \wedge F.\left(\alpha F^{\dagger}X + d\right) + w \qquad (19)$$

Defining $D = Fd$ in (19), then it can be articulated as in the following equation.

$$R = \alpha \wedge F + \wedge D + w \qquad (20)$$

Since Λ is diagonal, it can perform symbol-by-symbol detection. The difficulty is that D might in general be correlated with X. The preceding correlation could originate from d in the linearisation model.

4.3.1 Particle Filter Equalisation Algorithm

The MIMO structure uses redundant signals for different channel conditions, helping in reducing sampling dimension and aiding in implementing the IC strategy. A proposition suggests exploiting redundant information for frequency-selective MIMO fading channels with Gaussian distributed coefficients and noise.

Proposition: For frequency-selective MIMO fading channels, assume the channel fading coefficient $h_{ij,t}(i = 1,2, \ldots., n_T, j = 1,2, \ldots\ldots, n_R, t = 1,2, \ldots.)$ and noise v to be the Gaussian distribution, the transmit signal $s(i)(i = 1,2, \ldots.)^2$ is taken from a finite alphabet set$P_r(S|Y)$ to denote the probability of transmitted signal S under the received signal$Y$. For the given$\big(s(i), h_{ij,t}\big), \big(s(m), h_{mj,t}\big)$, if $\left|\left|h_{ij,t}\right|\right| > \left|\left|h_{mj,t}\right|\right|$, then it satisfies the following equation.

$$P_r(s(i)|y) > P_r(s(m)|y), \frac{P_r\big(s(i)|y\big)}{P_r\big(s(m)|y\big)} \propto \frac{\left|\left|h_{ij,t}\right|\right|}{\left|\left|h_{mj,t}\right|\right|} \quad (21)$$

Proof: Consider the received signal as (here take two signals, for example, more than two signals can be deduced by analogy).

$$y = s(i)h_{ij,t} + s(m)h_{mj,t} + v \quad (22)$$

Where, $h_{*j,t} \sim N(u, \alpha^2), v \sim N(0, \sigma^2), s(i),$ and $s(m)$ are transmitted with identical power,$\left|\left|s(i)\right|\right| = \left|\left|s(m)\right|\right|$ Assume $s(i)$ is the signal to be equalised and $s(m)$ is the interference, then $s(i)h_{ij,t}$ is expressed as follows.

$$s(i)h_{ij,t} = y - s(m)h_{mj,t} - v \quad (23)$$

As $\|h_{ij,t}\| > \left|\left|h_{mj,t}\right|\right|$, thus $\left|\left|s(i)h_{ij,t}\right|\right| = ||s(m)h_{mj,t}||$ Moreover, the SINR of $s(i)$ can be defined as $SINR_1 = 101\text{g}\left(\frac{h^T{}_{ij,t}\, h_{ij,t}}{h^T{}_{mj,t}\, h_{mj,t} + \sigma^2}\right)$ for $h * jt$ is constant, therefore the SINR can be further expressed as $SINR_2 = 10\ lg\ (\frac{||s(m)h_{mj,t}||}{\left|\left|s(i)h_{ij,t}\right|\right| + \sigma^2})$, obviously $SINR_1 > SINR_2$, therefore, $P_r(s(i)|y) > P_r(s(m)|y)$ is obtained.

In PF scheme, particles with weights decide probabilistically. Weight calculation involves normalisation of symbols.

4.4 Channel Capacity Enhancement Using SWIPT

In this section, the study has investigated the combined power splitting and PA optimisation to achieve the highest possible data rate in mm-wave M-MIMO-NOMA schemes with SWIPT. For the occurrence of both inter -and intra-group interferences

in the MIMO-NOMA system. Table 1 illustrates the SWIPT algorithm of the mm-wave M-MIMO-NOMA system.

Table 1. Algorithm for SWIPT and Power Transfer

Algorithm 1: mm-Wave M-MIMO-NOMA Organisations With SWIPT

Input: Number of UEs**:** $K > N^{RF}$**,** Number of RF chains: N^{RF}**,** Channel Matrix:$H = [h_1, h_2, \dots\dots, h_k]$**,** Optimised User Grouping:$\{\widehat{g_1}, \widehat{g_1}, \dots\dots, \widehat{g_G},\}$**,** Amount of BS antennas: N**,** Optimal analogue RF precoding: F^{RF}**,** Number of Quantisation bits: B

Output: Optimal Baseband precoding: F^{BB}

Set the phase: $\wedge = \left\{\frac{2\pi n}{2^B}, n = 0,1, \dots., 2^{B-1}\right\}$

$\bar{H} = H^H F^{RF}$

$\tilde{H}=[\bar{H}]_{.\hat{g}_1}$

$\hat{F}^{BB} = \tilde{H}^H(\tilde{H}\tilde{H}^H)^{-1}$

$\hat{F}^{BB} = \left[\frac{\hat{f}^{BB}{}_1}{f_1^{BB*}}, \frac{\hat{f}^{BB}{}_1}{f_2^{BB*}}, \dots\dots \frac{\hat{f}^{BB}{}_{NRF}}{f_{NRF}^{BB*}}, \right]$

Where $f_n^{BB*} = repmat(||F^{RF} f_n^{BB*}||_2, N^{RF}, 1) \vee n$

Initialise baseband precoding: $F^{BB} = 0^{NRF \times K}$

$[F^{BB}].\hat{g}_1 = \hat{F}^{BB}$

for Loop: g=1 to G

$\wedge = nonzeros([\wedge]_{\hat{g}_g})^T$

for m=2 to $|\wedge|$

$F^{BB}(:, \wedge_n) = [F^{BB}]:, \hat{g}_g$

end for

end for

Source: Adapted from (Hassan et al.,2023) algorithm builds upon the framework presented in Previous Work for mm-Wave M-MIMO-NOMA with SWIPT.

The intended EH restrictions and the communication power constraint requirements.

$$\max_{\{p_{g,m}\},\{\beta_m\}} R_{sum}\{p_{g,m}\},\{\beta_m\} \quad (24)$$

$$s.t. \sum_{g=1}^{G} \sum_{m=1}^{|S_g|} p_{g,m} \leq P_T \quad (25)$$

$$0 \leq \beta_m \leq 1 \vee m \quad (26)$$

$$p_{g,m} \geq 0 \vee g, m \quad (27)$$

$$P_{g,m}^{EH} \geq P_{g,m}^{req} \quad (28)$$

As a consequence of the objective function and the coupling of the multiple variables, the optimisation issue of the attainable data rate is neither convex nor linear because of the objective function.

5. Experimentation and Results Discussion

Spectral efficiency in given spectrum is the sum rate achieved, while Energy Efficiency (EE) is the ratio of total power consumed to the sum rate obtained. There are differences in propagation properties between legacy/conventional cellular systems and mmWave M-MIMO networks.

Table 2. Simulation System Configuration

MATLAB	Version R202a
Operation System	Windows 10 Home
Memory Capacity	6GB DDR3
Processor	Intel Core i5 @ 3.5GHz
Simulation Time	10.190 seconds

Source: Simulation setup for Table 2 of the information details the simulation environment and isn't presented as data or an outcome. For consistency with other tables that might have source notes that can include a brief one.

The simulation system configuration of the suggested work is shown in Table 2. Subsequently, the proposed technique is evaluated and tested under the Matlab R2022a software. The planned work operates under Windows 10 Home and its memory capacity is 6GB DDR3. Additionally, it utilises an Intel Core i5 @ 3.5GHz processor, and the simulation time of the work is 10.190 seconds.

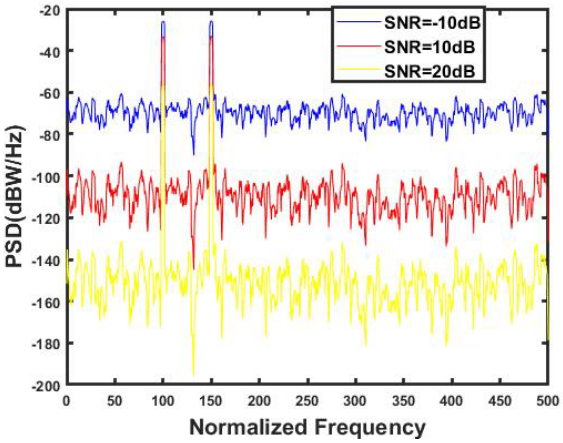

Figure 2. Analytical PSD for NOMA-OFDM Signals

Source: This MATLAB-generated image displays a signal's frequency spectrum, showing its constituent frequencies. The y-axis represents the power spectral density, while the x-axis is normalised frequency.

Figure 2 shows the analytical PSD for NOMA-OFDM signals. The PSD of these two modulation techniques shows the frequency localisation of the NOMA-OFDM. It is measured based on the normalised frequency, which consists of SNR values of -10dB, 10dB, and 20dB. Here, when the SNR values increase, the PSD becomes narrower.

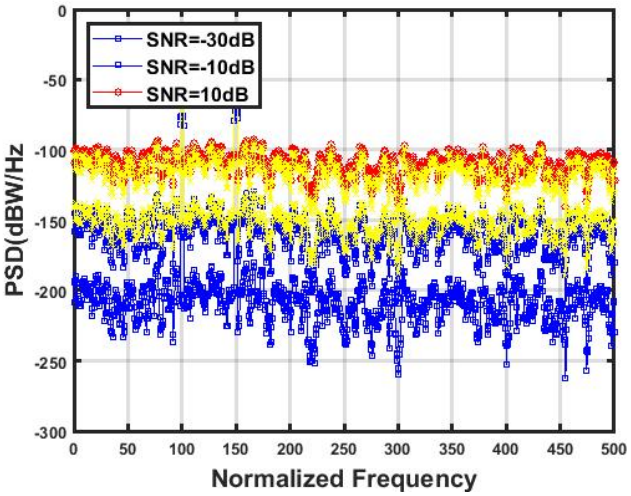

Figure 3. PSD of Received GFDM for Several SNR Rates

Source: This MATLAB-generated image displays a signal's frequency spectrum, showing its constituent frequencies. It shows the frequency spectrum of a signal, which reveals the signal's constituent frequencies.

The FBMC, GFDM, and NOMA signals exhibit an elevated power spectral density correlated to their signal-to-noise ratios, as illustrated in Figure 3. These signals were specifically crafted at SNR levels of (-30) dB, (-10) dB, and 10 dB. The difference between and signal in cases of significant sound alteration is difficult to tell (for -10 dB and -30 dB SNR).

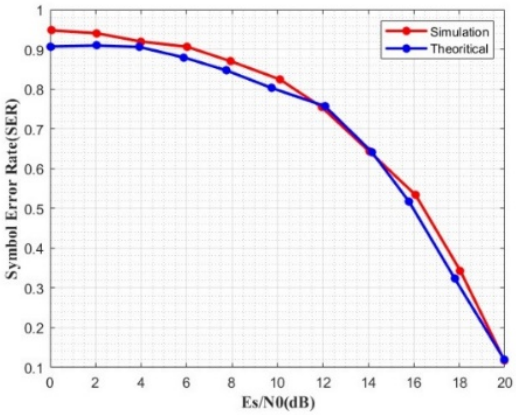

Figure 4. Symbol Error Rate Curve

Source: This MATLAB-generated image displays a graph that compares theoretical SER with simulation results. The x-axis is Ex/N0 (energy per bit over noise power spectral density) in dB. The y-axis is the symbol error rate.

Figure 4 offers the intended and replicated SER with given CFO Δf for Rayleigh flat fading channels and frequency selective channels with 8 taps exponential influence interruption profile ($D = 7$) respectively. The outcomes show that the methodology can very correctly estimate the simulative show if the power delayed profile of fading channels and CFO is understood.

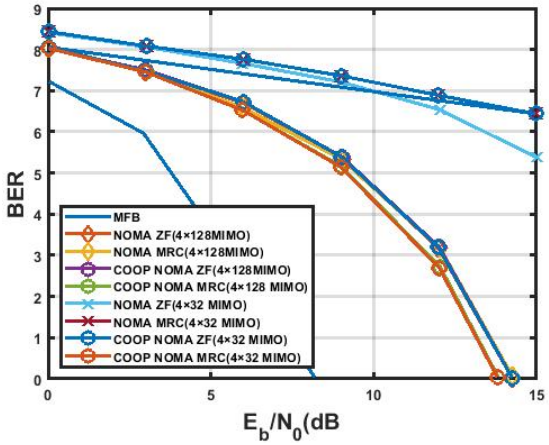

Figure 5. BER Results for 5 NOMA Users with Powers

Source: This MATLAB-generated image displays the specific graph that depicts performance in a millimetre wave (mmWave) channel, according to the text labels.

In Figure 5, we can see a comparison between the 4-way 128 MIMO and 4-way 32 MIMO systems, each with 5 NOMA users and varying received power levels [2 1 0.5 4 8] (where 2 represents the reference user's power). This demonstrates that increasing MIMO diversity can effectively counteract the performance decrease caused by a larger number of NOMA users.

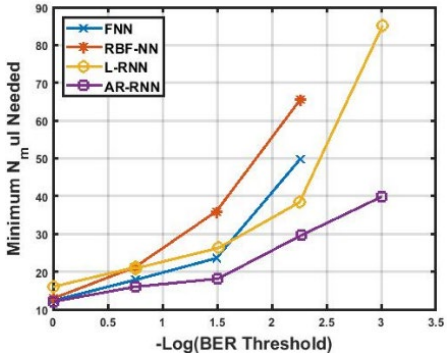

Figure 6. Minimum Number Required Under Different BER

Source: This visual representation produced by MATLAB illustrates the essential nutrients required for a biological function. Time is represented on the x-axis, while the y-axis displays the quantity of nutrients needed.

Since AR-RNN shows a much better concert than F-NN with the same size, n [0] and n [1] could be reduced to save CC for a secure BER threshold. However, for L-RNN, the limited BER presentation improvement may not be neutralised by reducing n [0] or n [1], consequently can observe an intersection of the F-NN and L-RNN in Figure 6.

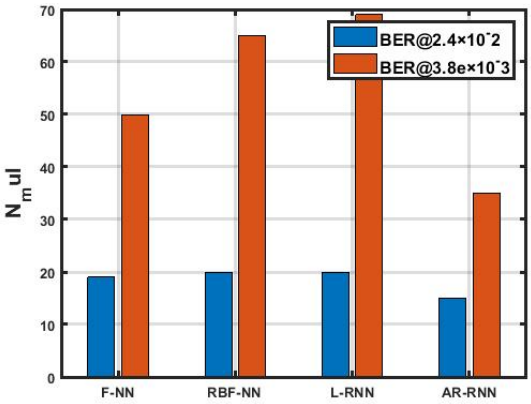

Figure 7. Minimum Number for Hard-Decision/Soft-Decision BER Thresholds
Source: This MATLAB-generated image displays the BER Thresholds for Hard and Soft decisions of the thresholds, as signified in the graph section.

The minimum N_{mul} requirement for hard-decision/soft-decision BER thresholds is shown in Figure 7. To be more specific, both the 20% soft-decision and 7% hard-conclusion FEC thresholds are considered. For BER recital under the 7% hard-judgment FEC threshold (3.8×10−3), an AR-RNN with only 7 inputs and 3 HNs can work well, which brings in the least CC among all 4 types of NNs.

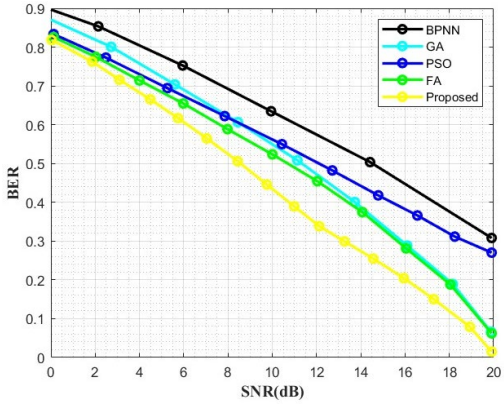

Figure 8. Comparison Analysis Graph for BET with SNR
Source: This MATLAB-generated image display shows the cost of the algorithm changes as it runs for more iterations. The proposed algorithm seems to achieve a lower cost than other algorithms after a certain number of iterations.

Figure 8 investigates the BER analysis of the presented FFA-RBFNN technique with other existing techniques under varying SNR. From this figure, it is identified that the FFA-RBFNN technique has resulted in an effective outcome by offering the lowest SNR. For instance, with the SNR of 16dB, the FFA-RBFNN technique has obtained a minimal BER of 10-6.3.

Table 3. Performance Values for the Suggested Work

Techniques	SNR
BPNN	0.308 dB
GA	0.262 dB
PSO	0.066 dB
FA	0.053 dB
Proposed	0.008 dB

Source: The comparison is taken from the findings of the validating results for the anticipated method of existing techniques.

Table 3 compares the techniques, with BPNN having the best SNR, followed by GA, PSO, FA, and the proposed method with the lowest SNR. This indicates their effectiveness in signal processing. The proposed method evaluated and yielded the lowest SNR of 0.008 dB among all the techniques, indicating the least effective signal processing or the lowest signal quality in this particular comparison.

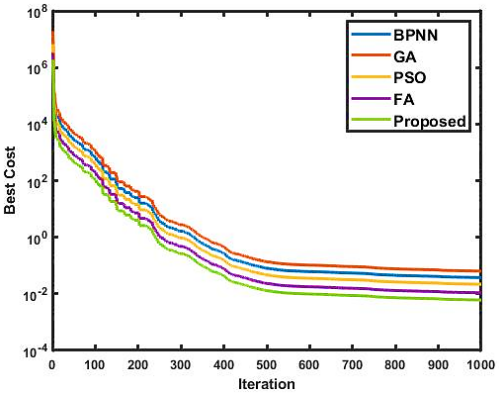

Figure 9. Best Cost Function at Each Iteration

Source: This MATLAB-generated image displays shows the cost of the algorithm changes as it runs for more iterations. The proposed algorithm seems to achieve a lower cost than other algorithms after a certain number of iterations.

Figure 9 depicts the best Cost Function (CF) results based on the number of repetitions as 1000. The proposed approach is pitted against the established techniques of BPNN, GA, PSO, and FA for comparison. The first iteration may be greater than that at the initialisation for initial spatial filters that have no constraint toward the DOA of the target.

Table 4. Comparison Table for BER and CF

	BPNN	GA	PSO	FA	Proposed
BER	$10^{-4.8}$	$10^{-6.4}$	$10^{-5.2}$	$10^{-5.7}$	$10^{-6.3}$
Best CF	$10^{-1.2}$	$10^{-1.05}$	$10^{-1.8}$	$10^{-1.95}$	$10^{-2.2}$
FFA-RBFNN for N_{mul} /BER					
Maximum N_{mul} Needed	**FNN**	**RBF-NN**	**L-RNN**	**AR-RNN**	**FFA-RBFNN**
0.5	15	18	20	13	14
1	19	25	22	16	15
1.5	23	35	25	19	20
2	40	52	34	25	25
2.5	-	-	50	32	30
3	-	-	75	40	38

Source: The comparison is taken from the findings of the validating results for the anticipated method of existing techniques.

The comparison table for BER, best CF and FFA-RBFNN for Nmul /BER are portrayed in Table 4. In this study, we evaluate the expected approach against established techniques such as BPNN, GA, PSO, and FA, while also contrasting NN with alternative models such as FNN, RBF-NN, L-RNN, and AR-RNN. Compared to these existing methods, the future method produces lower values for BER and CF that are 10-6.3 and 10-2.2. Therefore, the recital of the obtainable process is improved.

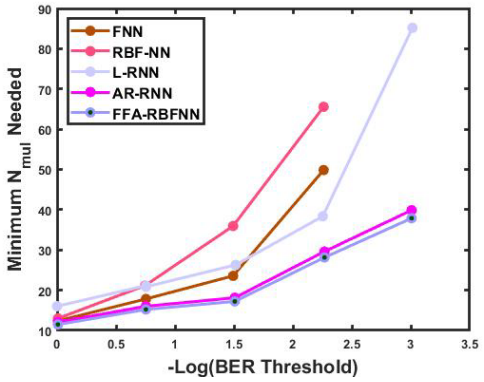

Figure 10. Comparison Results for BER Threshold

Source: This MATLAB-generated image displays the minimum number of nitrogen types needed to treat aluminium nitrate, likely referring to a chemical process. The x-axis shows and the y-axis shows Minimum N mul Needed.

Figure 10 shows the BER comparison, with the proposed method consistently outperforming the others, maintaining lower BER thresholds as the maximum Nmul increases. BER threshold values span from 10-5.2 (Nmul = 0.5) to 10-1.8 (Nmul = 2). The innovative approach consistently outperforms other methods, maintaining lower BER thresholds even as the maximum Nmul is increased. The BER threshold varies from 10-6.3 (Nmul = 0.5) to 10-2.2 (Nmul = 2).

6. Research Conclusions

In this work, DL-NOMA-OFDM is analytically characterised by the existence of nonlinear properties caused by an HPA. The article studied the grouping of mMIMO and mmWave equipment for spectral efficiencies and energy, throughput, and capacity of the CS. In exploring the OFDM-NOMA network with NLD in both the UL and DL, factors such as user data rates, total capacity, system fairness, and individual user BER are all critically analysed. A precise estimation of the power spectral density (PSD) and Signal-To-Distortion Ratio (SDR) is created for every user, demonstrating that the alternative method confirms a comprehensive optimal signal-to-oise ratio (SNR).

This system is designed and implemented using MATLAB software. The CC is increased as the power is allotted efficiently among the users that are present in the systems. The algorithm's effectiveness in meeting the 5G standards is then demonstrated through a back-to-back data transmission experiment. The combination of cognitive radio (CR) and NOMA can offer higher SE and higher data rates in future wireless networks. The results of the reproduction study showed that implementing the proposed PA strategies can enhance performance when compared to the current system, thus demonstrating the efficacy of the planned methods.

References

[1] Aini, I.R., Handayani, P. (2021), *Spectral Efficiency of MU-Massive MIMO System for Perfect and Imperfect CSI Condition. In 2021 International Seminar on Intelligent Technology and Its Applications (ISITIA) IEEE,* 23-28.

[2] Ali, D.M., Yahya, Z.Z. (2022), *Flexible Sub-Bands F-OFDM Configured for Spectrum Efficiency Enhancement in 5G System. J. Commun.,* 17(3), 203-209.

[3] Butenko, V.V., Devyatkin, E.E., Ivankovich, M.V., Lobov, E.M., Varlamov, V.O. (2021), *Modeling the Physical Layer of Advanced Radio Access Systems with Increased Spectral Efficiency Based on FBMC Technology. In 2021 Systems of Signal Synchronization, Generating and Processing in Telecommunications (SYNCHROINFO) IEEE,* 1-5.

[4] Ding, L., Zou, D., Wang, W., Li, F., Li, Z. (2021), *Generation of faster-than-Nyquist coherent optical DFT-spread OFDM signals with high-baud and high-order modulations. Optical Fiber Technology,* 64, 102526.

[5] Harish Kumar, G., Rao, P.T. (2022), *An energy efficiency perceptive on MIMO-OFDM systems using hybrid fruit fly-based salp swarm optimization technique. Concurrency and Computation: Practice and Experience,* 35(1), e7416.

[6] Hei, Y., Liu, X., Li, W., Wang, S., Huo, M. (2022), *Energy-and Spectral-Efficiency Tradeoff in Nonlinear OFDM System of Visible Light Communications. Journal of Lightwave Technology,* 40(7), 1921-1929.

[7] Hossain, M.N. (2022), *Performance evaluation of MIMO DFT-Spread WR-OFDM system for spectrum efficiency and power efficiency*. *Journal of Information and Telecommunication,* 1-17.

[8] Li, M., Liu, X. (2022), *Particle filtering-based iterative identification methods for a class of nonlinear systems with interval-varying measurements. International Journal of Control, Automation and Systems,* 20(7), 2239-2248.

[9] Liang, S., Tong, J., Ping, L. (2018), *On iterative compensation of clipping distortion in OFDM systems. IEEE Wireless Communications Letters,* 8(2), 436-439.

[10] Mal, Y., Yuan, Z., Yu, G., Xia, S., Hu, L. (2022*), A Spectrum Efficient Waveform Integrating OFDM and FMCW for Joint Communications and Sensing. In 2022 IEEE International Conference on Communications Workshops (ICC Workshops) IEEE,* 475-479.

[11] Sidiq, S., Sheikh, J.A., Mustafa, F., Malik, B.A., Sofi, I.B. (2022), *A New Genetic Algorithm Bio-inspired Based Impartial Evaluation of UFMC and GFDM Under Diverse Window Constraints. Arabian Journal for Science and Engineering,* 1-12.

[12] Singh, S.K., Kumar, A. (2022, April), *Modified design of STBC Encoder for reducing Non-Linear distortions in OFDM Channel Estimation. In 2022 Second International Conference on Advances in Electrical, Computing, Communication and Sustainable Technologies (ICAECT) IEEE,* 1-5.

[13] Singh, S.K., Kumar, A. (2022, April), *Modified design of STBC Encoder for reducing Non-Linear distortions in OFDM Channel Estimation. In 2022 Second International Conference on Advances in Electrical, Computing, Communication and Sustainable Technologies (ICAECT) IEEE,* 1-5.

[14] Unnisa, N., Tatineni, M. (2022), *Adaptive deep learning strategy with red deer algorithm for sparse channel estimation and hybrid precoding in millimeter wave massive MIMO-OFDM systems. Wireless Personal Communications,* 122(4), 3019-3051.

[15] Vaigandla, K.K., Benita, J. (2022), *Novel Algorithm for Nonlinear Distortion Reduction Based on Clipping and Compressive Sensing in OFDM/OQAM System. Sat.* 2, 10.

[16] Vaigandla, K.K., Benita, J. (2022), *Study and analysis of multi carrier modulation techniques–FBMC and OFDM. Materials Today: Proceedings, 58*, 52-56.

[17] Vieira, L.C., Ozan, W., Mitchell, J., Darwazeh, I. (2022), *Modeling and compensation of nonlinear distortion in direct-detection optical Fast-OFDM systems. In 2022 13th International Symposium on Communication Systems, Networks and Digital Signal Processing (CSNDSP) IEEE,* 168-173.

[18] Wu, Y., Han, C., Chen, Z. (2022), *DFT-Spread Orthogonal Time Frequency Space System with Superimposed Pilots for Terahertz Integrated Sensing and Communication. arXiv preprint arXiv:2202.10035*.

[19] Yang, Y., Dang, S., Wen, M., Guizani, M. (2021), *Millimeter Wave MIMO-OFDM with Index Modulation: A Pareto Paradigm on Spectral-Energy Efficiency Trade-Off. IEEE Transactions on Wireless Communications*, 20(10), 6371-6386.

[20] Zhang, L., Jiang, R., Tang, X., Chen, Z., Chen, J., Wang, H. (2021), *A simplified post equalizer for mitigating the nonlinear distortion in sipm-based ofdm-vlc system. IEEE Photonics Journal,* 14(1), 1-7.

[21] Zhang, Y., Li, Y., Fang, X., Sha, X., Feng, Y., Wang, W. (2022), *Towards spectral efficiency enhancement for IoT-aided smart transportation: a compressive OFDM transmission and regularized recovery approach. EURASIP Journal on Advances in Signal Processing,* 2022(1), 1-16.

[22] Zheng, S., Wu, S., Li, H., Jiang, C., Jing, X. (2021, October), *Deep Learning-Aided Receiver Against Nonlinear Distortion of HPA in OFDM Systems. In 2021 13th International Conference on Wireless Communications and Signal Processing (WCSP) IEEE*, 1-6.

[23] [23] Rahman, M.H., Sejan, M.A.S., Aziz, M.A., You, Y.H., Song, H.K. (2023), *HyDNN: A Hybrid Deep Learning Framework Based Multiuser Uplink Channel Estimation and Signal Detection for NOMA-OFDM System*. *IEEE Access*.